



HAL
open science

Circularly Polarized Luminescence and Circular Dichroism of Bichromophoric Difluoroboron- β -diketonates: Inversion and Enhanced Chirality Based on Spatial Arrangements and Self-Assembly

Joy Ann Panis, Marine Louis, Arnaud Brosseau, Shouhei Katao, Florencio de los Reyes, Takuya Nakashima, Rémi Métivier, Clémence Allain, Tsuyoshi Kawai

► To cite this version:

Joy Ann Panis, Marine Louis, Arnaud Brosseau, Shouhei Katao, Florencio de los Reyes, et al.. Circularly Polarized Luminescence and Circular Dichroism of Bichromophoric Difluoroboron- β -diketonates: Inversion and Enhanced Chirality Based on Spatial Arrangements and Self-Assembly. *Chemistry - A European Journal*, 2022, 28 (44), 10.1002/chem.202201012 . hal-03818463

HAL Id: hal-03818463

<https://hal.science/hal-03818463>

Submitted on 17 Oct 2022

HAL is a multi-disciplinary open access archive for the deposit and dissemination of scientific research documents, whether they are published or not. The documents may come from teaching and research institutions in France or abroad, or from public or private research centers.

L'archive ouverte pluridisciplinaire **HAL**, est destinée au dépôt et à la diffusion de documents scientifiques de niveau recherche, publiés ou non, émanant des établissements d'enseignement et de recherche français ou étrangers, des laboratoires publics ou privés.

Circularly Polarized Luminescence and Circular Dichroism of Bichromophoric Difluoroboron- β -diketonates: Inversion and Enhanced Chirality Based on Spatial Arrangements and Self-Assembly

Joy Ann Panis,^[a, b] Marine Louis,^[a] Arnaud Brosseau,^[b] Shouhei Katao,^[a] Florencio de los Reyes,^[a] Takuya Nakashima,^[a] Rémi Métivier,^{*,[b]} Clémence Allain,^{*,[b]} and Tsuyoshi Kawai^{*,[a]}

[a] J. A. Panis, Prof. M. Louis, S. Katao, F. de los Reyes, Prof. T. Nakashima, Prof. T. Kawai
Photonic and Reactive Molecular Science Laboratory, Division of Materials Science, Nara Institute of Science and Technology, Ikoma Nara (Japan)

E-mail: tkawai@ms.naist.jp

[b] J. A. Panis, A. Brosseau, Dr. R. Métivier, Dr. C. Allain

Université Paris-Saclay, ENS Paris-Saclay, CNRS, PPSM, 91190 Gif-sur-Yvette (France)

E-mail: remi.metivier@ens-paris-saclay.fr

clemence.allain@ens-paris-saclay.fr

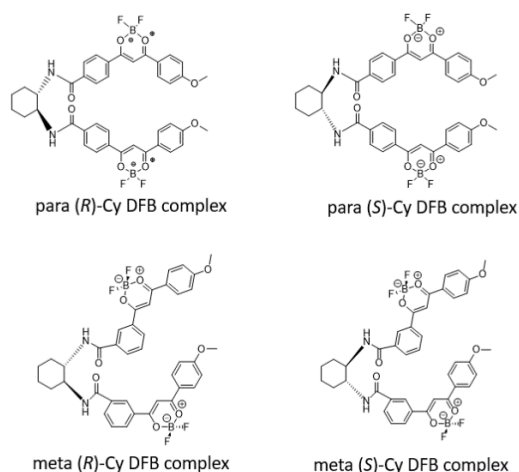
Supporting information for this article is available on the WWW under <https://doi.org/10.1002/chem.202201012>

Abstract: We synthesized two bichromophoric difluoroboron- β -diketonates (DFB) connected in para and meta positions by using cyclohexane diamine as a chiral bridge (**para and meta (R/S)-CyDFB**). TD-DFT calculations revealed that the variation in connectivity of the DFB units leads to different spatial arrangements and a chirality inversion of the bichromophoric DFB. Higher gabs values were obtained in **(R/S)-CyDFB** connected in para as compared to meta position. Aggregation of **para (R/S)-CyDFB** in mixture of solvents increase the glum values as compared to its monomeric form. Ultrasonication and heating induced the formation of highly ordered nano-helical wires of **para (R/S)-CyDFB** that increased the glum values to 0.015. On the other hand, **meta (R/S)- CyDFB** failed to form highly ordered self-assembled wires due to hindered H-binding sites. These observations indicate that the chiroptical properties of DFB bi-chromophore system can be modulated with self-assembly and spatial arrangement of the chromophores.

Introduction

Chiral substances display various specific features in their chemical reactivity, molecular recognition and chiroptical properties. Circularly polarized luminescence, CPL, is one of the typical chiroptical features of chiral substances, which have accumulated substantial interest from viewpoints of mechanistic understanding in early studies.[1–3] Functional applications of CPL active substances have also been proposed such as chiral molecular sensors and emitters for future OLED displays.[4–7] They encouraged some chemists to develop CPL active substances with large CPL dissymmetry factor, *glum*. In terms of *glum*, chiral Eu (III) complexes have been extensively studied, indicating *glum* > 1.0.[8,9] While simple organic molecules display limited *glum* values, strategic molecular design have been recently introduced for systematic enhancement of *glum* values. CPL nature of organic molecules and coordination substances in self-organized supramolecular aggregates have been extensively studied, in which long-range exciton coupling is expected to enhance chiroptical activity.[10–12] Aggregation induced emission (AIE) of some chiral organic molecules has also been reported for enhanced CPL capability.[13,14] As one of the most promising fluorophores for the supramolecular approaches, we have been recently focusing on difluoroboron- β -diketonate (DFB) complexes because of the high quantum yield in both solid and solution states,[15] high Stokes shift and sensitivity to stimuli such as mechanical stress[15–17] and presence of organic vapors.[18] Typical BF₂ units may promote specific inter-molecular association. It has been previously reported that DFB complex bearing chiral amido group displays a good CPL signal and response to mechanical stress in

solid state but showed weak CPL signals in monomeric state.[19] However, supramolecular aggregates of long range self-assembly based on this chromophore remain to be investigated. In the present study, we reported two new bichromophoric DFB compounds with chiral cyclohexane diamine bridge (Figure 1). Different solvents systems lead to different aggregated forms and photophysical and chiroptical properties. We show that both the geometry of the bichromophore (relative orientations of the DFB units toward the chiral diamine, Figure 2) and the solvent systems strongly influence the chiroptical



properties.

Figure 1. Chemical structures of DFB derivatives studied here.

Results and Discussion

Synthesis

The target compound (Figure 1) **para (R/S)-CyDFB** was synthesized by Claisen condensation reaction of 4-methoxy acetophenone and dimethyl terephthalate forming β -diketonate. Saponification with LiOH converts ester to carboxylic group,[16] and this step was followed by peptidic coupling of *para (R/S)* cyclohexane diamine forming the bichromophoric ligand.[20] Finally, complexation of the bichromophore ligand using $\text{BF}_3(\text{OEt})_2$ yields a yellow powder of **para (R/S)-CyDFB** after purification. Characterizations with ^1H , ^{13}C NMR, and Spiral TOF mass spectrometry confirms the target compound. The same steps were used to synthesize the **meta (R/S)-CyDFB** but using dimethyl isophthalate in Claisen condensation reaction instead of dimethyl terephthalate (Figure S1–S2).

Photophysical properties in solution and TD-DFT calculations

Photophysical properties of **para** and **meta (S)-CyDFB** were first investigated in dichloromethane (DCM) wherein the compounds displayed a good solubility. Both compounds display a broad and intense absorption band centered at 390 nm. The molar absorption coefficient (ϵ) of **para (S)-CyDFB** was higher ($105,000 \text{ M}^{-1} \text{ cm}^{-1}$) than **meta (S)-CyDFB** ($72,000 \text{ M}^{-1} \text{ cm}^{-1}$) indicating a higher energy harvesting property. The fluorescence quantum yield of **para** and **meta (S)-CyDFB** in DCM are 0.67 and 0.64 respectively.

The absorption and emission spectra of **para** and **meta (S)- CyDFB** were measured with different solvent polarities (Figure S3). Absorption spectra for both compounds do not significantly shift ranging from 389 nm to 398 nm for **para (S)- CyDFB** and 385 nm to 393 nm for **meta (S)-CyDFB** indicating less interactions of their ground state to solvent molecules.[21] Emissions for **para (S)-CyDFB** displayed maximum wavelength at 440 nm, 446 nm 443 nm and 444 nm in chloroform, DCM, THF and toluene while **meta (S)-CyDFB** displayed at 436 nm, 442 nm, 436 nm and 440 nm respectively. However, there are noticeable shifts of emissions in polar solvents such as DMF and acetonitrile indicating a weak intramolecular charge transfer nature in the excited state with the presence of methoxy

as electron donating group.[22] Lippert-Mataga plot (Figure S4–S5) showed a linear correlation between the solvent orientation polarizability and the Stokes shift, excluding toluene for which specific aromatic solute to solvent interactions may occur.[23]

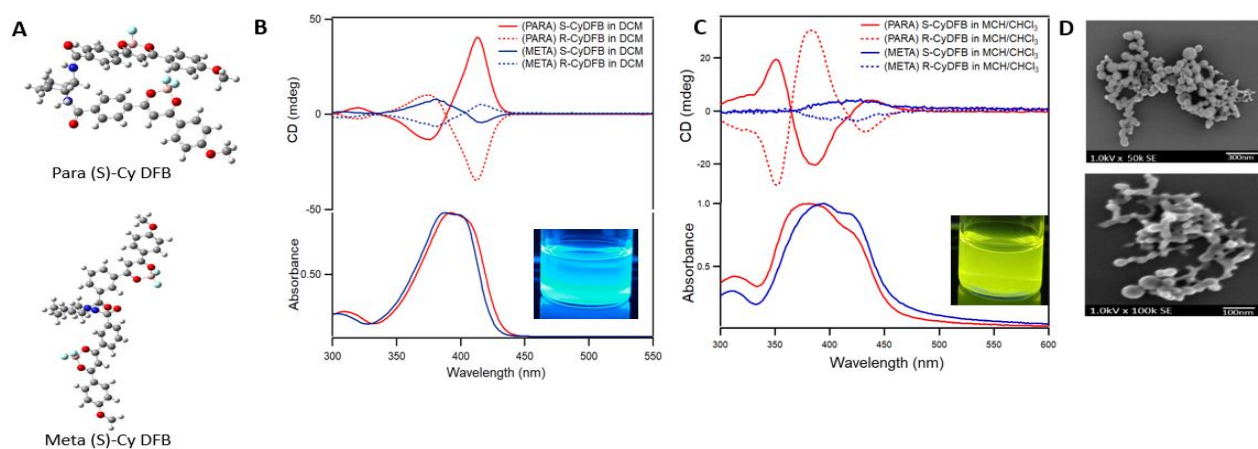


Figure 2. A) Optimized geometries of **para** and **meta (S)-CyDFB** based on DFT calculation with IEFPCM (DCM) solvation method. B) CD spectra and normalized absorbance of **para CyDFB** and **meta CyDFB** in DCM (3.5×10^{-5} M), insert is photograph of a DCM solution of **para CyDFB** under 365 nm excitation. C) CD spectra and normalized absorbance of **para CyDFB** and **meta CyDFB** in (29 : 1) MCH:Chloroform (3.5×10^{-5} M) insert is photograph of a (29 : 1) MCH:Chloroform solution of **para CyDFB** under 365 nm excitation, indicating fluorescent clear solution with low level of extinction signal in the range 500–600 nm (bottom). D) SEM images of aggregates of **para CyDFB** (top) and **meta CyDFB** (bottom).

Time-resolved spectroscopy measurements were conducted to gain insights to the emitting species in **para** and **meta (S)-CyDFB** in DCM solution. The decays were fitted with required satisfactory value of $X^2 < 1.2$ and the summary of decays are listed in Table 1. **Para (S)-CyDFB** exhibits a bi-exponential decay with decay time values $\tau_1 = 12$ ns ($a_1 = 0.01$) and $\tau_2 = 2.0$ ns ($a_2 = 0.99$) while **meta (S/R)-CyDFB** exhibited tri-exponential decay with decay time values $\tau_1 = 7$ ns ($a_1 = 0.02$) and $\tau_2 = 2$ ns ($a_2 = 0.70$) and $\tau_3 = 0.7$ ns ($a_3 = 0.27$) measured at emission wavelength of 463 nm (Table 1). For both compounds, the main contributions are from emitting species with decays around 2 ns which may be attributed to the individual DFB unit by comparison with related monomeric compounds.[19] Long decay times 12 ns for **para (S)-CyDFB** and 7 ns for **meta (S)-CyDFB** may be attributed to intramolecular exciton coupling between the two DFB units bridged by the cyclohexane diamine.

To understand the molecular electronic properties of the compounds, density functional theory (DFT) and time-dependent DFT (TDDFT) calculations were performed in Gaussian 16 program using the functional CAM B3LYP and basis set (6-31)+G(d,p) with IEFPCM (DCM) solvation method. Optimized ground state geometry revealed that **para (S)-CyDFB** in DCM have two non-equivalents DFB units (Figure 2A).

In the first DFB, dihedral angle of phenyl group connected through amide bond has dihedral angle of 27.4° with respect to amide plane which is more twisted than the second DFB moiety with an angle 4.8° . Phenyl rings of the first DFB moiety has dihedral angle of 13.3° and 1.19° with respect to the difluoroboron β -diketonate plane while the phenyl rings of second DFB unit have dihedral angles of 24.9° and 6.97° respectively. The two DFB groups in **para (S)-CyDFB** were in proximity and overlapped their phenyl group attached in amide bonds (Figure S10). Single crystal analysis of **para (S)-CyDFB** showed a slight variation in arrangement of DFB moieties mainly because of presence of intermolecular interactions in crystals while the DFT was calculated in monomeric form (Figure 4A).

On the other hand, optimized geometry of **meta (S)-CyDFB** showed that the DFB groups are in equatorial position where both are headed to the opposite sides (Figure 2A). The phenyl rings connected

to amide group has dihedral angle of 18.4° and 18.9° with respect to amide plane. In the first DFB moiety, phenyl rings have dihedral angle of 13.5° and 7.6° with respect to difluoro boron β -diketonate plane while in the second DFB moiety, phenyl rings have dihedral angle of 9.9° and 8.2° with respect to difluoro boron β -diketonate plane (Figure S10).

The electronic transitions and corresponding involved molecular orbitals of **para** and **meta (S)-CyDFB** were calculated by time-dependent DFT (TD-DFT). The results showed that there are multiple molecular orbitals involved in each transition (Figures S11–S12). Natural transition orbitals (NTO) were also calculated to clearly demonstrate the electronic transitions involving multiple molecular orbitals. Both transitions showed a π - π^* character with a slight shift of electron density from methoxy towards the β -diketonate group (Figure S11–S12). This explains the weak solvatochromism property of both **para** and **meta-(S/R)-CyDFB**.

CD and CPL properties in DCM solution and aggregated forms in MCH/chloroform solution

Chirality of monomeric compounds in the ground state were studied by circular dichroism (CD) measurement of both **para** and **meta (S/R)-CyDFB** compounds dissolved in DCM. CD spectra of **para (S/R)-CyDFB** enantiomers show mirror images with positive Cotton effect for *S* enantiomer while negative cotton effect for *R* enantiomer. Interestingly, **meta (S/R) CyDFB** display an opposite Cotton effect measured at the same wavelength as **para (S/R)-CyDFB** (Figure 2B). The observed Cotton effect signs in Figure 2B for both **para** and **metaCyDFB** are in good agreement with the theoretical CD spectra from TD-DFT (Figure S13).

Table 1. Emission decay time constant (τ), pre-exponential factor (a) and fraction of intensity (f) of monomers in DCM of para and meta (S)-CyDFB ($\lambda_{exc}=390$ nm, $\lambda_{em}=463$ nm) (1), aggregates in MCH/CHCl ₃ of para and meta (S)-CyDFB ($\lambda_{exc}=390$ nm, $\lambda_{em}=550$ nm) (2), and gels in toluene of para (S)-CyDFB measured ($\lambda_{em}=390$ nm, $\lambda_{em}=450$ nm and 550 nm) (3).				
Sample	τ_1 (ns), (a_1, f_1)	τ_2 (ns), (a_2, f_2)	τ_3 (ns), (a_3, f_3)	τ_4 (ns), (a_4, f_4)
1 para (S)-CyDFB (monomers in DCM)				
($\lambda_{em}=463$ nm)	12.2, (0.01, 0.03)	2.06, (0.99, 0.97)	–	–
meta (S)-CyDFB (monomers in DCM)				
($\lambda_{em}=463$ nm)	7.0, (0.02, 0.06)	2.4, (0.70, 0.84)	0.7, (0.27, 0.10)	–
2 para (S)-CyDFB (aggregates MCH/CHCl₃)				
($\lambda_{em}=550$ nm)	40.5, (0.72, 0.90)	14.7, (0.21, 0.10)	1.6, (0.07, 0.00)	–
meta (S)-CyDFB (aggregates MCH/CHCl₃)				
($\lambda_{em}=550$ nm)	40.9, (0.33, 0.70)	17.0, (0.27, 0.24)	2.7, (0.40, 0.06)	–
3 para (S)-CyDFB (gels in toluene)				
($\lambda_{em}=450$ nm)	11.5, (0.00, 0.3)	2.1, (0.72, 0.89)	0.5, (0.27, 0.08)	–
($\lambda_{em}=550$ nm)	35.5, (0.42, 0.91)	12.3, (0.04, 0.03)	2.3, (0.35, 0.05)	0.6, (0.19, 0.01)

As shown in the DFT optimized geometry, variation in connectivity of **para** and **meta** leads to different spatial arrangement of DFB units. **Para (S/R)-CyDFB** units are in axial position and the DFB groups are more aligned and overlapped with one aromatic ring. In contrast, the **meta** derivative favors the equatorial position and rearranged the DFB groups towards the opposite sides preventing interactions of two DFB units. Notably, CD spectra of bichromophoric DFB in **para** position showed more intense CD response and displayed twice the dissymmetry factor with $|gabs|$ value of 4×10^{-4} as compared

with DFB in meta position with $|g_{abs}|$ value of 2×10^{-4} (Figure 2B). Higher $|g_{abs}|$ value may be due to shorter distance of DFB units in para position causing excitonic coupling between the DFB units. Moreover, degree of overlap between the chromophores and the configurations of DFB units in DCM have directed the inversion of chirality.[24]

The measurements of photophysical properties were extended to self-assembled aggregates of **para** and **meta (S/R)-CyDFB** in a mixture of chloroform and methylcyclohexane (MCH) and chloroform (29:1) at concentration 3.5×10^{-5} M. The solution turns from bright blue emission in monomeric form (DCM) to yellow emission (Figures 2B and C) in mixture of MCH and chloroform (29 : 1) under UV light. This is accompanied by broadening of absorbance as compared with the monomeric form. SEM images showed a randomly connected spherical aggregates both in para and meta derivatives (Figure 2D). Like the monomeric form, CD spectra of **para (S/R)-CyDFB** aggregates displayed mirror images for (R) and (S) enantiomers with formation of new band at 430 nm displaying an opposite sign of more intense band at 385 nm (Figure 2C). These new bands correspond to the CD signals of newly formed absorbing species in aggregated form.

Interestingly, random aggregates formed by interacting units of **para (S/R)-CyDFB** showed an enhanced $|g_{abs}|$ values as compared to its monomeric form. Further increase in concentration from 3.5×10^{-5} M to 1.0×10^{-4} M displayed a decrease in dissymmetry factor from $|g_{abs}|$ value of 1.0×10^{-3} to $|g_{abs}|$ value of 3.0×10^{-4} . This is due to formation of bigger aggregates forming precipitation in higher concentration, which suggests low reliability in the latter value. As compared with the aggregates formed with **para (R/S)-CyDFB**, CD spectra of **meta (R/S)-CyDFB** have broader but weaker bands between 360 nm-460 nm. Newly formed bands in aggregated form of **para** and **meta** displayed an opposite sign of Cotton effect to its corresponding monomeric form. In contrast to enhancement of $|g_{abs}|$ values of **para**, **meta (R/S)-CyDFB** did not show any significant enhancement in dissymmetry factor upon formation of aggregates which remains $|g_{abs}|$ value of ca. 2.0×10^{-4} at concentration of 3.5×10^{-5} M.

Circularly polarized luminescence (CPL) measurements provided more evidence in chiroptical properties of **meta** and **para (R/S)-CyDFB** in their excited states. The $|g_{lum}|$ values of both para and meta isomers in monomeric form are too low to be reliably analyzed by the instrument (Figure S7A). This seems reasonable as the lowest $|g_{lum}|$ of our lab-designed machine is about 1×10^{-3} , which is not sufficient to characterize those as low as 2.0×10^{-4} . Meanwhile, the aggregated form of **para (R/S)-CyDFB** compounds notably showed a mirror image of R and S enantiomers and has $|g_{lum}|$ value of around 4.0×10^{-3} measured at 530 nm which corresponds to the emission from aggregates (Figures 3A and B). This clearly showed that the significant increase in $|g_{lum}|$ was attributed to the intermolecular excitonic coupling between DFB units in chiral aggregates, which should operate over 4 or more DFB units.[25] In contrast, the meta isomer displayed no significant CPL activity in both monomeric and the aggregated forms, which is attributable to less CPL activity to be detected in our system (Figure S7B). These results clearly demonstrate significant difference in the intramolecular and intermolecular excitonic coupling between DFB units of two these isomers.

To further understand the changes in dissymmetry factors in MCH rich solution, fluorescence decays were measured by TCSPC at $\lambda_{em}=550$ nm for both **para** and **meta (S)-CyDFB**. **Para (S)-CyDFB** aggregates exhibited tri-exponential decay with decay times at $\tau_1=40.5$ ns ($a_1=0.72$), $\tau_2=14.7$ ns ($a_2=0.21$) and $\tau_3=1.6$ ns ($a_3=0.07$). Likewise, **meta (S)-CyDFB** aggregates also displayed a tri-exponential decays with decay times at $\tau_1=40.8$ ns ($a_1=0.33$), $\tau_2=16.9$ ns ($a_2=0.27$) and $\tau_3=2.7$ ns ($a_3=0.40$) (Table1) (Figure S8).

Noticeably, the pre-exponential factor of decays at 40 ns in **para-CyDFB** is more than twice the pre-exponential in the meta isomer. This is in contrast with the short-lived species at around 2 ns which has higher pre-exponential factors in metaaggregates (40 %) but has low pre-exponential factor in para (7%).

The predominant decays of long-lived emitting species with decays at around 40 ns and 15–17 ns formed through intermolecular and intramolecular excitonic coupling may explain the enhanced chiroptical properties of para as compared with meta. These results also suggest rather minor and random biand multi-chromophoric coupling in the aggregated meta-isomer.

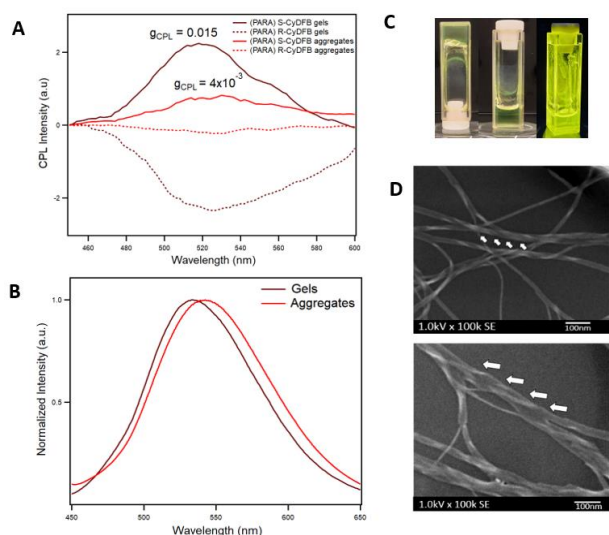


Figure 3. A) CPL Spectra of **para (R/S) CyDFB** gels formed in toluene (solid and broken dark red lines) and aggregates formed in MCH/CHCl₃ (solid and broken red lines). B) Normalized emission of **para (R/S)-CyDFB** gels (solid dark red line) and aggregates in (29 : 1) MCH/CHCl₃ (solid red line). C) Gels formed in toluene as shown in inverted vials at room light and under 365 nm UV source and D) SEM images of nanowires **para (S)-** (top) and **(R)-** (bottom) **CyDFB** obtained from gels.

Formation of organogels

Formation of **para (R/S)-CyDFB** organogels were observed in mixture of DCM and toluene (50 : 50) stimulated by ultrasonication followed by heating at 40 °C for 10 mins. The organogels were formed after 144 h of slow evaporation of DCM at room temperature. Pure toluene assisted with ultrasonication and heating formed a mixture of opaque aggregates and gels due to poor solubility of compounds in pure toluene. The presence of DCM in the solvent system balanced the solubility-precipitation of compounds and assisted the formation of thermodynamically stable organogels driven by π - π and hydrogen bonding.[26] The formation of gels is confirmed by stable inversion of test tube method. (Figure 3C).

Morphology of nanowires were observed after deposition and drying of organogels under vacuum (xerogels). SEM images of xerogels (Figure 3D) shows the formation of extended nanofibers with thickness ranging from 5 nm–15 nm. The single **para (S)-CyDFB** unit has molecular length around 1.8 nm as measured from the optimized structure calculated with DFT, hence it indicates that fibers formed are not one-dimensional but composed of multiple intertwined fibers which is evident in the images (Figure 3D). To gain more insights in the molecular arrangement, single crystal structure of **para (S)-CyDFB** complex was determined from a crystal obtained by slow solvent evaporation using DCM as solvent. Crystal structure revealed that the bichromophoric units has various side-to-side interactions involving fluorine atoms to the methoxy as well as Hatom of the adjacent DFB units via CH/F hydrogen bonding as shown in Hirshfeld surface analysis (Figure 4B).[27] Moreover, extending the structures from top to bottom shows the π - π stacking between the extended fibers owing to H-bonding (Figure 4A). It was clearly shown that C=O and NH from amide were mainly involved in hydrogen bonding. Diffraction patterns of xerogels obtained from powder XRD coincided with the simulated patterns from CIF file, suggesting that the nanowires have similar stacking with the crystal structures (Figure S13).

Simulated packing structures of bichromophoric units were obtained through Materials Studio 7.0 program using COMPASSII force field. The hydrogen bonding observed in crystal structure through amide group is also present in simulated packing but differs mainly in twisting of DFB group (Figure 4C). Notably, the proposed calculated structures of nanowires displayed a periodical single and double hydrogen bonding every four bichromophoric units leading to twisting of onedimension wires. DFB units were also bent downward as seen in the top DFB units and slightly reversing the bending towards the upward direction as seen in the last DFB unit located at the bottom part of the model. This possibility of one-dimensional twisting based on the proposed packing may explain the intertwining of fibers as observed in SEM images. Moreover, formation of nanowires through amides and carbonyl hydrogen bonding is in good agreement with the previous studies of self- assembled nanohelical wires involving cyclohexane diamine as the chiral backbone moiety.[25,28–30]

Photophysical properties and CPL of organogels

The emission spectra were monitored upon formation of organogels and initially, it displayed two emission bands at around 450 nm and 550 nm. The emission around 450 nm was attributed to the monomeric form while the emission at 550 nm (Figure S6).

TCSPC measurements of organogels provided more insights to the nature of emitters in nanowires. Table 1 shows that the long-live emitting species with decay-times $\tau_1=35$ ns ($a_1=0.42$) and is from the self-assembly which immediately formed after cooling down the solution at room temperature. Disappearance of emission at 430 nm after 144 h indicated that most of bichromophoric units were assembled into the helical nanowires $\tau_2=12.3$ ns ($a_2=0.04$) were prominent at longer wavelength but almost did not exist at 450 nm. These decays along with the shift in emission to higher wavelength suggests the formation of new emitting species through intramolecular and intermolecular coupling of DFB units. Shorter decay was observed at 550 nm ($\tau_3=2.3$ ns, $a_3=0.35$) but more prominent at 450 nm ($\tau_2=2.1$ ns, $a_2=0.72$) which is attributed to the residual monomers in the toluene solution. CPL measurements of **para (R/S)-CyDFB** organogels exhibited g_{lumj} value of about 0.015 which is not fully reproducible due to stability of gels with long exposure to UV source during CPL measurements but relatively high values for organic molecules that usually ranges from 10^{-2} to 10^{-5} . [25] High g_{CPL} values were observed at the range 530 nm–550 nm, which suggests that these CPL signals correspond to the newly formed emitting species in the selfassembled nanowires (Figure 4C). This value has two orders of magnitude higher than its monomeric form and an order of magnitude higher than the random aggregates in MCH:CHCl₃ solution. Similarities in lifetimes and CPL signals observed at λ_{em} 500 nm–550 nm for aggregated form and organogels may indicate that emitting species with longer lifetimes are present for both assemblies formed through intermolecular interactions. Significantly intense CPL signal observed in the nanowires is probably due to the highly ordered arrangement of bichromophoric DFB units forming helical and intertwined fibers. Such arrangement promotes the long range cooperative excitonic coupling between the chromophores causing enhanced CPL signals.[10,25,28]

The same method for the formation of organogels were tested for **meta (R/S)-CyDFB** using different solvents such as cyclohexane, hexane, toluene, acetonitrile, DCM, chloroform, and mixtures of polar and non-polar solvents. Unlike with the para-isomer, the meta isomer showed no organogel in any of these solvents but rather precipitations occurred in both nonpolar and mixtures of solvents.

Molecular packing arrangements of nanowires in **paraCyDFB** compounds revealed that hydrogen bonding involving amide groups is crucial in the formation of chiral backbone in stacked bichromophoric units. Comparison of the orientation of meta and para in DFT optimized geometry showed that the orientation of DFB units of meta are causing hindrance or blocking to the amide group hence suppressing the formation hydrogen bonding between the adjacent DFB bichromophoric units.

Introduction of long alkyl chain may help to form molecular wires and liquid crystalline states in future molecules.[31]

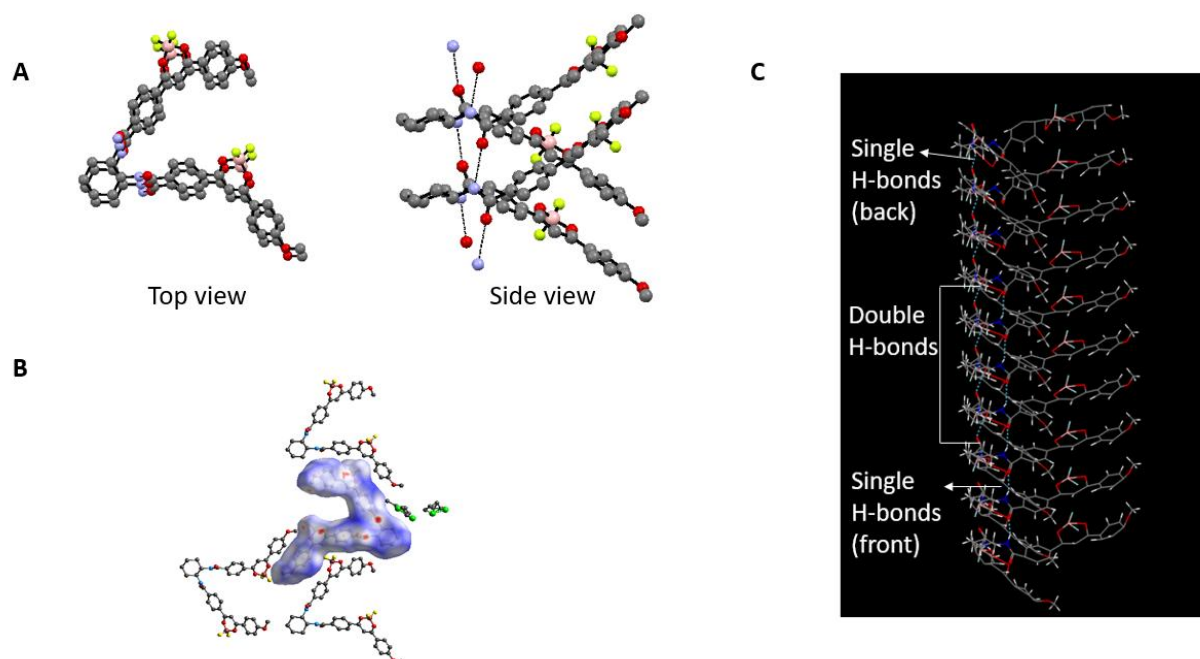


Figure 4. A) Top and side view of crystal packing induced by π - π stacking and hydrogen bonding of amide groups. B) Hirshfeld surface analysis and C) simulated packing structures of using Materials Studio 7.0.

Conclusion

We have synthesized two bichromophoric DFB complexes connected in para and meta position by using cyclohexanedia mine as chiral bridge moiety. The difference in connectivity of para and meta has led to variation in spatial arrangement of DFB units, hence exhibited inversed sign of Cotton effect. DFB complex in para position appeared to have stronger CD and CPL signals owing to the overlap and shorter distance of DFB units which favored the intramolecular coupling. CD and CPL signals in aggregated forms has increased as compared to the monomeric form accompanied by the existence of long-lived emitting species. This indicates prominent intermolecular and intramolecular excitonic coupling in the random aggregates. Moreover, para isomer formed nanowires in mixture of toluene and DCM solvent while the meta isomer failed to form nanowires showing that the spatial arrangements highly influenced the formation of π - π stacking and hydrogen bonding. Notably, the organogels displayed a glum value of about 0.015. The responsivity of these gels to various stimuli is currently being studied.

Experimental Section

Syntheses: Analytical reagents were purchased from Tokyo Chemical Industry Co., Ltd (TCI) and Sigma Aldrich and were used without further purification. The reactions were monitored using Merck TLC silica gel 60 F254 and visualized using UV lamp with wavelength 254 nm and 365 nm. ^1H , ^{13}C , ^{19}F and ^{11}B NMR analyses were recorded using 400 MHz, 500 MHz NMR JEOL JNM-ECX-500 and 600 MHz NMR JEOL JNM-ECA600. The reference used for the ^{19}F and ^{11}B NMR analyses is $\text{BF}_3 \cdot \text{O}(\text{C}_2\text{H}_5)_2$ in CDCl_3 . Mass was analyzed using high Bruker Autoflex II MALDI-TOF and JEOL MALDI SpiralTOF high resolution mass spectrometer.

Photophysical and chiroptical properties: All absorbance and emission measurements were conducted using spectroscopy grade solvent purchased from Fujifilm Wako Pure Chemicals Industries Ltd. without any purification. The absorbances were obtained using double beam UV-Vis Jasco V-760 and double beam spectrometers Cary 100. The emissions were measured using Jasco FP-8500, Horiba Jobin-Yvon spectrofluorometers Fluoromax FM3 and Fluorolog FL3-221 while the PLQY of aggregates

were measured using integrating sphere made by Hamamatsu and calculated using system software U6039-05 ver.3.2.1.

Time-dependent fluorescence decay: Fluorescence decay curves were obtained by the time-correlated single-photon counting (TCSPC) method. The setup is composed of a titanium sapphire Ti: Sa oscillator (Spectra Physics, Mai Tai HP) emitting pulses of 100 fs duration at 780 nm, 80 MHz frequency. The laser pulses then pass through a pulse picker which implements acousto-optic modulator to pick up specific pulse to reduce the repetition rate at 4 MHz. Then the signal was doubled at 390 nm by focalizing the laser in a non-linear SHG crystal (GWU Lasertechnik, UHG-23-PSK). Then the beam passes through the sample solution after adjusting the excitation power with an intensity attenuator filter wheel. Fluorescence photons were detected at 90° through a monochromator (CVI Laser Corporation, Digikröm CM110) and a polarizer at magic angle by means of a micro channel plate photomultiplier (Hamamatsu, MCP-PMT R3809 U-50), connected to a TCSPC module (Becker & Hickl, SPC-130-EMN). The instrumental response function was recorded before each decay measurement with a fwhm (full width at half-maximum) of ~25 ps. Time-correlated fluorescence decay data is finally processed and analyzed with the help of a software which implements the non-linear square method (Globals, Laboratory for Fluorescence Dynamics at the University of California, Irvine).

Circular dichroism (CD) and circularly polarized luminescence (CPL): CD spectra of monomeric and aggregated forms of **para** and **meta (R/S)-CyDFB** in chloroform and methylcyclohexane (MCH) rich solvents were measured using circular dichroism spectropolarimeter JASCO J-725 using nitrogen gas flow of 5 ml/min and controlled temperature using Peltier system. The CPL were measured using the lab-designed CPL system consisting of excitation laser at 375 nm, Hinds PEM-90 photoelastic modulator with frequency of 50KHz, Hamamatsu H7732 photomultiplier tube with signal amplifier, polarizing prism and Shimadzu monochromator (10 cm, single grating). The system was previously calibrated, and the detailed information has been discussed in previous manuscript.[32]

Calculations: Optimized geometry of **para** and **meta (S)-CyDFB** were calculated using CAM B3LYP functional and 6-31+ g (d,p) basis set including IEFPCM (DCM) solvation model. The energy transitions, molecular orbitals, simulated ECD, absorbance and oscillator strengths were calculated with TD-DFT using the same basis sets solvent models as the optimization. The calculation was conducted using Mésocentre” computing center of CentraleSupélec and École Normale Supérieure Paris-Saclay supported by CNRS and Région Île-deFrance.

Powder XRD and crystallography: Gels of **para (S)-CyDFB** were deposited on clean glassslides and dried under vacuum overnight to remove the solvents, also referred to as xerogels. The powder XRD patterns were recorded using Rigaku Smartlab9 kW using CuK α 1 monochromatization Ge220crystals. **Para (S)-CyDFB** crystals were obtained by slow evaporation process starting from a saturated DCM solution. Suitable single crystal was isolated and mounted in sample holder. X-ray diffractions were recorded using Rigaku Varimax Rapid RA Micro7 equipped with imaging plate detector monochromated Mo K α radiation at 103.15 K. The crystal structure and calculations were done using the system software Rigaku Crystal structure 3.8.1.

Deposition Number 2163664 (for **para (S)-CyDFB**) contains the supplementary crystallographic data for this paper. These data are provided free of charge by the joint Cambridge Crystallographic Data Centre and Fachinformationszentrum Karlsruhe Access Structures service.

UHR FESEM imaging: Sample for FESEM imaging were prepared by drop casting ~5–10 μ L of aggregated samples in methylcyclohexane/chloroform and gels in copper grid coated with thin layer of carbon for adhesion. The grids were dried under vacuum overnight to remove all the residual solvent prior to imaging. Ultrahigh-resolution field emission scanning electron microscopy (UHR FESEM) imaging was done using Hitachi SU9000 equipped with a secondary electron detector. The equipment

has a superior low-kV performance utilizing in-lens SEM optics and improved vacuum technology. The samples were run using acceleration voltage ranging from 1 to 5 kV.

Acknowledgements

This project had received funding from the European Research Council(ERC) under the European Unions Horizon 2020 research and innovation program (grant agreement No. 715757 MECHANO-FLUO to C.A.). We would like to acknowledge Nara Institute of Science and Technology, Division of Materials Science, Photonic and Reactive Molecular Laboratory and ENS-Paris Saclay Laboratoire de Photophysique et Photochimie Supramoléculaires et Macromoléculaires (PPSM) for the financial support. This work was performed using HPC resources from the “Mésocentre” computing center of CentraleSupélec and École Normale Supérieure Paris-Saclay supported by CNRS and Région Île-de-France (<http://mesocentre.centralesupelec.fr/>). We also thank the NAIST technical staffs, Ms. Y. Nishikawa and Mr. F. Asanoma, for their kind support on MS- and NMR-measurements. ML would also like to thank the NAIST Foundation for their financial support.

Conflict of Interest: The authors declare no conflict of interest.

Data Availability Statement

The data that support the findings of this study are available from the corresponding author upon reasonable request.

Keywords : bichromophores ; circularly polarized luminescence; circular dichroism; difluoroboron- β -diketonates ; self-assembly

References

- [1] K. Kogashi, T. Matsuno, S. Sato, H. Isobe, *Angew. Chem. Int. Ed.* **2019**, *58*, 7385–7389; *Angew. Chem.* **2019**, *131*, 7463–7467.
- [2] S. Sato, A. Yoshii, S. Takahashi, S. Furumi, M. Takeuchi, H. Isobe, *Proc. Natl. Acad. Sci. USA* **2017**, *114*, 13097–13101.
- [3] C. Yamamoto, Y. Okamoto, *BCSJ* **2004**, *77*, 227–257.
- [4] K. Dhbaibi, L. Favereau, J. Crassous, *Chem. Rev.* **2019**, *119*, 8846–8953.
- [5] N. Saleh, B. Moore, M. Srebro, N. Vanthuyne, L. Toupet, J. A. Williams, C. Roussel, K. K. Deol, G. Muller, J. Autschbach, J. Crassous, *Chem. Eur. J.* **2015**, *21*, 1673–1681.
- [6] L. Favereau, C. Quinton, C. Poriel, T. Roisnel, D. Jacquemin, J. Crassous, *J. Phys. Chem. Lett.* **2020**, *11*, 6426–6434.
- [7] M. Li, S. Li, D. Zhang, M. Cai, L. Duan, M. K. Fung, C. F. Chen, *Angew. Chem. Int. Ed.* **2018**, *57*, 2889–2893; *Angew. Chem.* **2018**, *130*, 2939–2943.
- [8] E. M. Sánchez-Carnerero, A. R. Agarrabeitia, F. Moreno, B. L. Maroto, G. Muller, M. J. Ortiz, S. de la Moya, *Chem. Eur. J.* **2015**, *21*, 13488–13500.
- [9] T. Goto, Y. Okazaki, M. Ueki, Y. Kuwahara, M. Takafuji, R. Oda, H. Ihara, *Angew. Chem. Int. Ed.* **2017**, *56*, 2989–2993; *Angew. Chem.* **2017**, *129*, 3035–3039.
- [10] R. Tempelaar, A. Stradomska, J. Knoester, F. C. Spano, *J. Phys. Chem. B* **2011**, *115*, 10592–10603.
- [11] T. Ikeda, M. Takayama, J. Kumar, T. Kawai, T. Haino, *Dalton Trans.* **2015**, *44*, 13156–13162.
- [12] H. Jintoku, M.-T. Kao, A. Del Guerso, Y. Yoshigashima, T. Masunaga, M. Takafuji, H. Ihara, *J. Mater. Chem. C.* **2015**, *3*, 5970–5975.
- [13] T. Ikeda, T. Masuda, T. Hirao, J. Yuasa, H. Tsumatori, T. Kawai, T. Haino, *Chem. Commun.* **2012**, *48*, 6025–6027.

- [14] T. Kawai, K. Kawamura, H. Tsumatori, M. Ishikawa, M. Naito, M. Fujiki, T. Nakashima, *ChemPhysChem* **2007**, *8*, 1465–1468.
- [15] H. Zhang, P.-Z. Chen, L.-Y. Niu, Q.-Z. Yang, *Mater. Chem. Front.* **2020**, *4*, 285–291.
- [16] M. Louis, A. Brosseau, R. Guillot, F. Ito, C. Allain, R. Métivier, *J. Phys. Chem. C* **2017**, *121*, 15897–15907.
- [17] N. D. Nguyen, G. Zhang, J. Lu, A. E. Sherman, C. L. Fraser, *J. Mater. Chem.* **2011**, *21*, 8409–8415.
- [18] L. Zhai, M. Liu, P. Xue, J. Sun, P. Gong, Z. Zhang, J. Sun, R. Lu, *J. Mater. Chem. C* **2016**, *4*, 7939–7947.
- [19] M. Louis, R. Sathy, J. Kumar, S. Katao, R. Guillot, T. Nakashima, C. Allain, T. Kawai, R. Métivier, *Chem. Sci.* **2019**, *10*, 843–847.
- [20] J. Kumar, T. Nakashima, T. Kawai, *J. Phys. Chem. Lett.* **2015**, *6*, 3445–3452.
- [21] P. Galer, R. C. Korošec, M. Vidmar, B. Šket, *J. Am. Chem. Soc.* **2014**, *136*, 7383–7394.
- [22] P.-Z. Chen, L.-Y. Niu, Y.-Z. Chen, Q.-Z. Yang, *Coord. Chem. Rev.* **2017**, *350*, 196–216.
- [23] J. M. Živković, I. M. Stanković, D. B. Ninković, S. D. Zarić, *Cryst. Growth Des.* **2020**, *20*, 1025–1034.
- [24] J. Kumar, T. Nakashima, T. Kawai, *Langmuir* **2014**, *30*, 6030–6037.
- [25] J. Kumar, T. Nakashima, H. Tsumatori, T. Kawai, *J. Phys. Chem. Lett.* **2014**, *6*, 316–321.
- [26] X. Zhang, R. Lu, J. Jia, X. Liu, P. Xue, D. Xu, H. Zhou, *Chem. Commun.* **2010**, *46*, 8419–8421.
- [27] P. R. Spackman, M. J. Turner, J. J. McKinnon, S. K. Wolff, D. J. Grimwood, D. Jayatilaka, M. A. Spackman, *J. Appl. Crystallogr.* **2021**, *54*, 1006–1011.
- [28] J. Kumar, T. Nakashima, H. Tsumatori, M. Mori, M. Naito, T. Kawai, *Chem. Eur. J.* **2013**, *19*, 14090–14097.
- [29] R. Sathy, J. Kumar, R. Métivier, M. Louis, K. Nakatani, N. M. T. Mecheri, A. Subhakumari, K. G. Thomas, T. Kawai, T. Nakashima, *Angew. Chem. Int. Ed.* **2017**, *56*, 15053–15057; *Angew. Chem.* **2019**, *129*, 15249–15253.
- [30] R. Sathy, R. Métivier, A. Brosseau, T. Kawai, T. Nakashima, *J. Phys. Chem. Lett.* **2018**, *9*, 4516–4521.
- [31] H. Yamamoto, T. Inagaki, J. Park, S. Yoshida, K. Kaneko, T. Hanasaki, K. Akagi, *Macromolecules* **2021**, *54*, 8977–8986.
- [32] J. Yuasa, T. Ohno, K. Miyata, H. Tsumatori, Y. Hasegawa, T. Kawai, *J. Am. Chem. Soc.* **2011**, *133*, 9892–9902.
- [33] Gaussian 16, Revision, M. J. Frisch, G. W. Trucks, H. B. Schlegel, G. E. Scuseria, M. A. Robb, J. R. Cheeseman, G. Scalmani, V. Barone, G. A. Petersson, H. Nakatsuji, X. Li, M. Caricato, A. V. Marenich, J. Bloino, B. G. Janesko, R. Gomperts, B. Mennucci, H. P. Hratchian, J. V. Ortiz, A. F. Izmaylov, J. L. Sonnenberg, D. Williams-Young, F. Ding, F. Lipparini, F. Egidi, J. Goings, B. Peng, A. Petrone, T. Henderson, D. Ranasinghe, V. G. Zakrzewski, J. Gao, N. Rega, G. Zheng, W. Liang, M. Hada, M. Ehara, K. Toyota, R. Fukuda, J. Hasegawa, M. Ishida, T. Nakajima, Y. Honda, O. Kitao, H. Nakai, T. Vreven, K. Throssell, J. A. Montgomery, Jr., J. E. Peralta, F. Ogliaro, M. J. Bearpark, J. J. Heyd, E. N. Brothers, K. N. Kudin, V. N. Staroverov, T. A. Keith, R. Kobayashi, J. Normand, K. Raghavachari, A. P. Rendell, J. C. Burant, S. S. Iyengar, J. Tomasi, M. Cossi, J. M. Millam, M. Klene, C. Adamo, R. Cammi, J. W. Ochterski, R. L. Martin, K. Morokuma, O. Farkas, J. B. Foresman, and D. J. Fox, Gaussian, Inc., Wallingford CT, **2016**.

Manuscript received: April 1, 2022 ; Accepted manuscript online: May 30, 2022